Grid Synchronization of Doubly-fed Induction Generator Using Integral Variable Structure Control

Si Zhe Chen, Norbert C. Cheung, *Senior Member, IEEE*, Ka Chung Wong, and Jie Wu

***Abstract*—This paper proposes a novel direct voltage control scheme, using integral variable structure control to synchronize a doubly fed induction generator (DFIG)-based wind energy conversion system (WECS) to the grid. The proposed scheme directly controls the stator terminal voltage of the DFIG to track the grid voltage without current control loop; hence, the structure of controller is simplified. The control scheme includes parametric uncertainty and external disturbances into the formed design procedure; hence, the proposed scheme has better robustness than existing synchronization methods. Both computer simulation and hardware implementation results are presented to demonstrate the advantages of the proposed scheme.**

***Index Terms*—DFIG, direct voltage control, integral variable structure control, synchronization, wind energy.**

NOMENCLATURE

$u_{\rm dg}, u_{\rm qg}$	Direct and quadrature grid voltage.
$u_{\rm ds}, u_{\rm qs}$	Direct and quadrature stator winding voltage.
$u_{\rm dr}, u_{\rm qr}$	Direct and quadrature rotor winding voltage.
$i_{\rm dr}, i_{\rm qr}$	Direct and quadrature rotor winding current.
$\lambda_{\rm ds}, \lambda_{\rm qs}$	Direct and quadrature stator flux.
$\lambda_{\rm dr}, \lambda_{\rm qr}$	Direct and quadrature rotor flux.
$\omega_g, \omega_r, \omega_s$	Grid, rotor, and slip angular frequency.
R_r	Rotor winding resistance.
L_m, L_r	Magnetizing and rotor self-inductance.
p_n	Number of pole pairs.
Δ	Parameter deviation or signal noise.

Superscripts

*	Reference value.
sen	Sensor signal included noise.

Subscripts

g, s, r	Grid, stator, and rotor.
d, q	Synchronous d–q-axis.
max, min	Upper and lower limits of the parameter.
0	Nominal value of parameter.

Manuscript received January 30, 2009. First published October 23, 2009; current version published November 20, 2009. This work was supported by the National Natural Science Foundation of China under Grant 60534040 and by The Hong Kong Polytechnic University under Grant G-U497. Paper no. TEC-00033-2009.

S. Z. Chen is with the College of Electric Power, South China University of Technology, Guangzhou 510640, China, and also with the Department of Electrical Engineering, The Hong Kong Polytechnic University, Kowloon, Hong Kong (e-mail: cszscut@126.com).

J. Wu is with the College of Electric Power, South China University of Technology, Guangzhou 510640, China (e-mail: epjiewu@scut.edu.cn).

N. C. Cheung and K. C. Wong are with the Department of Electrical Engineering, The Hong Kong Polytechnic University, Kowloon, Hong Kong (e-mail: norbert.cheung@polyu.edu.hk; eekcwong@polyu.edu.hk).

Digital Object Identifier 10.1109/TEC.2009.2025316

I. INTRODUCTION

DUE to the gradual depletion of fossil energy resources and the increasingly concern for environmental pollution, it has become increasingly important for all countries of the world to develop renewable energy for the sustainable development of human society. Wind energy is a major form of renewable energy. Wind energy conversion system (WECS) can be divided into fixed speed type and variable speed type. Compared to fixed speed WECS, variable speed WECS has the advantages of maximizing the output power, reducing mechanical stresses, improving the power quality, and increasing the transient stability margin of the electrical grids [1], [2]. Variable speed WECS can further be subdivided into two types: one based on synchronous generators and the other based on doubly fed induction generators (DFIG). Compared with synchronous generators, DFIG are more suitable for high-power application, because only a portion of the generated energy needs to be processed by the power electronics converters [3]. Hence, DFIG-based WECS have dominated the high-power wind turbine market.

The control of DFIG is achieved by changing the magnitude, frequency, and phase of the rotor voltages or rotor currents. In the early years, most DFIG systems employed either naturally commutated dc-link converters or cycloconverters in the rotor circuits, which resulted in expensive dc-link choke, extra commutation circuit, and low-frequency current harmonics. Some researchers used a back-to-back pulse width modulation (PWM) converter in the rotor circuit to overcome these drawbacks [4]. The modeling and control strategies of the DFIG have been widely reported in [4], [5]. In these references, the rotor converter is controlled using field-oriented control (FOC) in the stator flux vector reference frame. The rotor current is decomposed into a parallel component and an orthogonal component, which are independently regulated for controlling the reactive powers and machine torques of the DFIG. In spite of the number of papers related to DFIG, there are relatively few publications, describing the synchronization of the DFIG to the power grids [6]–[9].

However, soft and fast synchronization is an important issue, because it enables the DFIG to be connected to the grid with minimum impact on the WECS and the grid. Another important application of fast synchronization is reclosing the DFIG

with the grid immediately after grid faults, in order to provide voltage support and frequency support to the grid, which will enhance the fault ride through (FRT) ability of WECS [10]. In [6], only the direct and quadrature rotor currents are controlled for synchronization. The lack of voltage feedback might result in significant differences between the stator and grid voltages and hence cause impact at the time of connecting. Cascaded approaches are used in [7], [8], in which the inner loop is used to control rotor current, and the outer loop is implemented to minimize the voltage differences before the generator is connected to the power grid. In [9], the stator voltage is directly controlled instead of passing through a chain of cascaded loops, which reduces the demand on the computation power and the number of parameters for tuning.

From control viewpoint, these approaches use state transformation after which the decoupling and linearization tasks can be performed easily. However, precise knowledge of the DFIG parameters is needed, which cannot be known exactly in practical since: the DFIG model is a simplified machine model; the DFIG parameters are normally obtained by identification procedures in which errors are always present; the DFIG parameters may vary with ambient temperature and exciting saturation. In recent years, a lot of research effort has been devoted to the application of variable structure control (VSC) techniques to power electronic equipment and electrical drives [11]–[15]. Interest in this control approach has emerged due to its potential for being insensitive to variations of system parameters and external disturbances with a minimum of implementation complexity.

This paper proposes a robust single-loop direct voltage control (DVC) scheme for synchronization. The stator voltage is directly controlled instead of passing through a chain of cascaded loops and hence the structure of controller is simplified. In order to enhance the robustness of the system against parametric uncertainty and external disturbances, the VSC with an integral action, so called integral variable structure control (IVSC) is introduced into the control loop. The paper is organized as follows. Sections II and III give the topology and mathematical model of the DFIG. Section IV simply describes the principle of IVSC. In Section V, the DVC for synchronization of DFIG-based WECS using IVSC is designed, and the parametric uncertainty and external disturbances are formally included. In Section VI and VII, simulation and experimental results are reported to validate the robustness of proposed scheme against parametric uncertainty and external disturbances.

II. Description of the DFIG System

The schematic diagram of the DFIG-based WECS is shown in Fig. 1. The DFIG is a wound rotor asynchronous machine mechanically coupled to a wind turbine. The stator winding is connected to the grid through a three-phase contactor. The rotor winding is connected to the grid through a bidirectional converter made up of two back-to-back three-phase full-bridge inverters (referred as rotor converter and grid converter). The rotor converter controls the voltage applied to the rotor winding of the DFIG. The grid converter controls the power flow between the dc-link and the grid to keep the voltage of capacitor in dc-link constant.

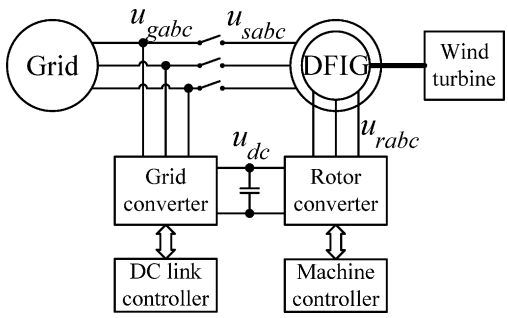

Fig. 1. DFIG-based WECS.

III. Mathematical Model

A. Mathematical Model of DFIG

The equations describing the operation of the DFIG before it is connected to the grid in a synchronous reference frame are

$$u_{\mathrm{ds}} = \frac{d\lambda_{\mathrm{ds}}}{dt} - \omega_g \lambda_{\mathrm{qs}} \tag{1}$$

$$u_{\mathrm{qs}} = \frac{d\lambda_{\mathrm{qs}}}{dt} + \omega_g \lambda_{\mathrm{ds}} \tag{2}$$

$$u_{\mathrm{dr}} = R_r i_{\mathrm{dr}} + \frac{d\lambda_{\mathrm{dr}}}{dt} - \omega_s \lambda_{\mathrm{qr}} \tag{3}$$

$$u_{\mathrm{qr}} = R_r i_{\mathrm{qr}} + \frac{d\lambda_{\mathrm{qr}}}{dt} + \omega_s \lambda_{\mathrm{dr}} \tag{4}$$

$$\lambda_{\mathrm{ds}} = L_m i_{\mathrm{dr}} \tag{5}$$

$$\lambda_{\mathrm{qs}} = L_m i_{\mathrm{qr}} \tag{6}$$

$$\lambda_{\mathrm{dr}} = L_r i_{\mathrm{dr}} \tag{7}$$

$$\lambda_{\mathrm{qr}} = L_r i_{\mathrm{qr}} \tag{8}$$

.

For the purpose to achieve direct voltage control, the direct relationship between the stator voltage and the rotor voltage will be developed. Substituting (7) and (8) into (3) and (4) and rearranging gives

$$\frac{di_{\mathrm{dr}}}{dt} = -\frac{R_r}{L_r} i_{\mathrm{dr}} + \frac{1}{L_r} u_{\mathrm{dr}} + \omega_s i_{\mathrm{qr}} \tag{9}$$

$$\frac{di_{\mathrm{qr}}}{dt} = -\frac{R_r}{L_r} i_{\mathrm{qr}} + \frac{1}{L_r} u_{\mathrm{qr}} - \omega_s i_{\mathrm{dr}}. \tag{10}$$

As the stator voltage and the stator flux have a multi-input–multioutput relationship, appropriate pairs of the voltage and flux components have to be identified to close the control loop correctly. Reference [9] used the relative gain array (RGA) methodology to calculate the degrees of relevance between the stator voltage and the stator flux and got the conclusion that the direct stator flux controls the quadrature voltage, whereas the quadrature stator flux controls the direct voltage, at steady state. Therefore, substituting (5) and (6) into (1) and (2) and

differentiating them with respect to time yields

$$\frac{du_{\mathrm{ds}}}{dt} = L_m \frac{d^2 i_{\mathrm{dr}}}{dt^2} - \omega_g L_m \frac{di_{\mathrm{qr}}}{dt} \tag{11}$$

$$\frac{du_{\mathrm{qs}}}{dt} = L_m \frac{d^2 i_{\mathrm{qr}}}{dt^2} + \omega_g L_m \frac{di_{\mathrm{dr}}}{dt}. \tag{12}$$

According to [9], the first terms in the right side of (11) and (12) can be regarded as disturbances. Substituting (10) into (11) and (9) into (12) gives

$$\frac{du_{\mathrm{ds}}}{dt} = -\frac{\omega_g L_m}{L_r} u_{\mathrm{qr}} + \frac{\omega_g L_m R_r}{L_r} i_{\mathrm{qr}} + \omega_g \omega_s L_m i_{\mathrm{dr}} + L_m \frac{d^2 i_{\mathrm{dr}}}{dt^2} \tag{13}$$

$$\frac{du_{\mathrm{qs}}}{dt} = \frac{\omega_g L_m}{L_r} u_{\mathrm{dr}} - \frac{\omega_g L_m R_r}{L_r} i_{\mathrm{dr}} + \omega_g \omega_s L_m i_{\mathrm{qr}} + L_m \frac{d^2 i_{\mathrm{qr}}}{dt^2}. \tag{14}$$

B. Parametric Uncertainty and External Disturbances

The machine parameters are obtained by identification experiments in which errors are unavoidable, and furthermore, these parameters may vary with ambient temperature and exciting saturation. Considering the uncertainties of the machine parameters, it is assumed that the parameters in (13) and (14) are bounded as follows

$$R_{r\,\min} < R_r = R_{r0} + \Delta R_r < R_{r\,\max}$$

$$L_{m\,\min} < L_m = L_{m0} + \Delta L_m < L_{m\,\max}$$

$$L_{r\,\min} < L_r = L_{r0} + \Delta L_r < L_{r\,\max}$$

where R_{r0}, L_{m0}, and L_{r0} denote the nominal values, and ΔR_r, ΔL_m, and ΔL_r denote the deviations.

In addition, there are unpredictable electromagnetic interference (EMI) in operating locale, which may cause unpredictable noises to the sensors in the WECS. So the real signals used by the controller are

$$i_{\mathrm{dqr}}^{\mathrm{sen}} = i_{\mathrm{dqr}} + \Delta i_{\mathrm{dqr}}$$

$$u_{\mathrm{dqs}}^{\mathrm{sen}} = u_{\mathrm{dqs}} + \Delta u_{\mathrm{dqs}}$$

$$u_{\mathrm{dqg}}^{\mathrm{sen}} = u_{\mathrm{dqg}} + \Delta u_{\mathrm{dqg}}$$

where $\Delta i_{\mathrm{dqr}}, \Delta u_{\mathrm{dqs}}$, and Δu_{dqg} denote the unknown noises.

IV. Variable Structure Control With Integral Action

The core idea of designing traditional VSC algorithms consists of enforcing sliding mode in a predefined sliding surface of the system state space. Once the system state reaches the sliding surface, the structure of the feedback loop is adaptively alter to slide the system state along the sliding surface. Hence, the system response depends only on the predefined sliding surface and remains insensitive to variations of system parameters and external disturbances. However, during the reaching phase, before sliding mode occurs, such insensitivity property is not guaranteed, which means the loss of the robustness in the transient state. Furthermore, in the practical implementation of the VSC, the sign function is often replaced by saturation function to reduce the chattering, which will result in undesirable steady-state error.

To deal with these problems, an integral action is introduced into traditional sliding mode scheme, which is so-called IVSC. By properly choosing the initial condition of the integrator, sliding mode can be established in the initial time instant without the reaching phase, implying that the invariance of the system to parametric uncertainty and external disturbances is guaranteed during the entire response. In addition, the integral action gives advantage of effectively minimizing the steady-state error caused by the saturation function.

V. Design of Proposed IVSC

Since the grid voltage is the only quantity not affected by the operation of the DFIG, the synchronous reference frame of the DFIG is aligned to the grid voltage. The q-axis of the synchronous reference frame is aligned to the grid voltage, and the d-axis is orthogonal to the grid voltage, so

$$u_{\mathrm{qg}} = V_g, \qquad u_{\mathrm{dg}} = 0$$

where V_g is the magnitude of the grid voltage.

The control objective is to control the stator direct and quadrature voltage to track the grid direct and quadrature voltage in the grid voltage reference frame, respectively, such that the stator voltage and grid voltage will have equal magnitude, frequency, and phase.

The sliding surfaces of the proposed IVSC for the stator direct and quadrature voltage control of DFIG are given as follows

$$s_d = x_d + c \int_{-\infty}^{t} x_d(z) dz_d = 0 \tag{15}$$

$$s_q = x_q + c \int_{-\infty}^{t} x_q(z) dz_q = 0 \tag{16}$$

where c is the coefficient of the sliding surface, z_d and z_q are the dummy variables for the integration, state variables x_d and x_q are the errors between the stator voltage and the grid voltage, respectively, and are defined as

$$x_d = u_{\mathrm{ds}} - u_{\mathrm{ds}}^* = u_{\mathrm{ds}} - u_{\mathrm{dg}} \tag{17}$$

$$x_q = u_{\mathrm{qs}}^* - u_{\mathrm{qs}} = u_{\mathrm{qg}} - u_{\mathrm{qs}}. \tag{18}$$

To guarantee the sliding mode in the whole transient state, the initial conditions of the integrators should be chosen as

$$I_{d0} = \frac{-x_{d0}}{c}, \qquad I_{q0} = \frac{-x_{q0}}{c}$$

where x_{d0} and x_{q0} are the initial conditions of x_d and x_q, I_{d0} and I_{q0} are the initial conditions of the integrators defined as

$$I_0 = \int_{-\infty}^{0} x(z) dz.$$

Hence at $t = 0$,

$$s_d(t_0) = x_{d0} + cI_{d0} = 0 \tag{19}$$

$$s_q(t_0) = x_{q0} + cI_{q0} = 0 \tag{20}$$

.

Equation (19) and (20) means that the system states are on the sliding surfaces in the initial time instant without the reaching phase, and the complete robustness can be obtained during the entire response.

The control inputs of the proposed scheme consists of the equivalent controls and switching controls and are given as

$$u_{\rm qr} = u_{\rm qr}^{\rm eq} + \Delta u_{\rm qr} \tag{21}$$

$$u_{\rm dr} = u_{\rm dr}^{\rm eq} + \Delta u_{\rm dr}. \tag{22}$$

The equivalent controls are used to control the nominal plant model, and the switching controls are added to ensure the desired performance despite parametric uncertainty and external disturbances.

By using the condition of the equivalent controls as $\dot{s}_{\rm dq} = 0$ [11], the equivalent controls are derived as

$$u_{\rm qr}^{\rm eq} = R_{r0} i_{\rm qr}^{\rm sen} + \omega_s L_{r0} i_{\rm dr}^{\rm sen} + \frac{L_{r0} c x_d^{\rm sen}}{\omega_g L_{m0}} - \frac{L_{r0}}{\omega_g L_{m0}} \frac{du_{\rm ds}^{*\rm sen}}{dt} \tag{23}$$

$$u_{\rm dr}^{\rm eq} = R_{r0} i_{\rm dr}^{\rm sen} - \omega_s L_{r0} i_{\rm qr}^{\rm sen} + \frac{L_{r0} c x_q^{\rm sen}}{\omega_g L_{m0}} + \frac{L_{r0}}{\omega_g L_{m0}} \frac{du_{\rm qs}^{*\rm sen}}{dt}. \tag{24}$$

The switching controls are given as

$$\Delta u_{\rm qr} = K_{d1} x_d^{\rm sen} sign(s_d x_d^{\rm sen}) + K_{d2} sign(s_d) \tag{25}$$

$$\Delta u_{\rm dr} = K_{q1} x_q^{\rm sen} sign(s_q x_q^{\rm sen}) + K_{q2} sign(s_q). \tag{26}$$

The constants K in (25) and (26) are determined by the well-known sliding-mode existence condition as

$$s_d \dot{s}_d < 0 \tag{27}$$

$$s_q \dot{s}_q < 0. \tag{28}$$

The constants to satisfy the inequality given in (27) are

$$K_{d1} > \max \left| \left(\frac{L_r L_{m0} - L_m L_{r0}}{\omega_g L_m L_{m0}} \right) c \right| \tag{29}$$

$$K_{d2} > \max \left| \frac{L_m L_{r0} - L_r L_{m0}}{\omega_g L_m L_{m0}} \frac{du_{\rm ds}^*}{dt} + (R_r - R_{r0}) i_{\rm qr} + \omega_s (L_r - L_{r0}) i_{\rm dr} + \frac{L_r}{\omega_g} \frac{d^2 i_{\rm dr}}{dt^2} - R_{r0} \Delta i_{\rm qr} - \omega_s L_{r0} \Delta i_{\rm dr} + \frac{L_{r0}}{\omega_g L_{m0}} \frac{d\Delta u_{\rm ds}^*}{dt} - \frac{L_r c \Delta x_d}{\omega_g L_m} \right|. \tag{30}$$

The constants to satisfy the inequality given in (28) are

$$K_{q1} > \max \left| \left(\frac{L_r L_{m0} - L_m L_{r0}}{\omega_g L_m L_{m0}} \right) c \right| \tag{31}$$

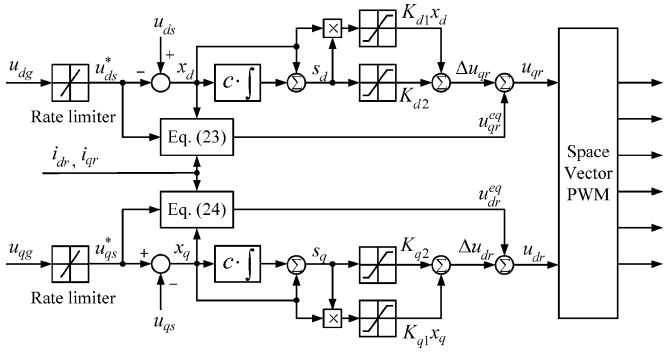

Fig. 2. Block diagram of proposed DVC scheme using IVSC.

$$K_{q2} > \max \left| \frac{L_r L_{m0} - L_m L_{r0}}{\omega_g L_m L_{m0}} \frac{du_{\rm qs}^*}{dt} + (R_r - R_{r0}) i_{\rm dr} + \omega_s (L_{r0} - L_r) i_{\rm qr} - \frac{L_r}{\omega_g} \frac{d^2 i_{\rm qr}}{dt^2} - R_{r0} \Delta i_{\rm dr} + L_{r0} \omega_s \Delta i_{\rm qr} - \frac{L_{r0}}{\omega_g L_{m0}} \frac{d\Delta u_{\rm qs}^*}{dt} - \frac{L_r c \Delta x_{\rm qr}}{\omega_g L_m} \right|. \tag{32}$$

In (30) and (32), $du_{\rm ds}^*/dt$ and $du_{\rm qs}^*/dt$ will be infinite if the reference values of stator voltage are abruptly changed, and K_{d2} and K_{q2} cannot be determined if parametric uncertainty is considered. Therefore, the rising and falling rates of input reference signals should be limited. Practically, in practical engineering implementations, rate limiters are also need to avoid large stress on mechanical and/or electrical components.

The switching actions in (25) and (26) will cause chattering phenomenon. The boundary layer solution can deal with this problem. The sign functions are replaced by saturation functions in a small vicinity of the sliding surface; hence, control discontinuities and switching action in the control loop is avoided. However, the boundary layer will cause steady-state errors. Fortunately, the integral action can deal with this problem. Fig. 2 shows the block diagram of the proposed scheme.

VI. Simulation Results

The proposed DVC scheme using IVSC is simulated with Matlab/Simulink. The rotor converter is modeled as a voltage source to simulate the state-averaged operation of the converter for saving simulation time. The machine parameters are shown in the Appendix. The rising and falling rate of stator quadrature voltage reference value is limited at ± 5000 V/s, and the rising and falling rate of stator direct voltage reference value is limited at ± 500 V/s. The value of sliding surface coefficient c is chosen as 80. To determine the switching control, the maximum bounds of the parameter errors are assumed as $-0.5R_{r0} < \Delta R_r < 0.5R_{r0}$, $-0.5L_{m0} < \Delta L_m < 0.5L_{m0}$, $-0.5L_{r0} < \Delta L_r < 0.5L_{r0}$, and the maximum bounds of unknown noises are assumed as 0.5% amplitude of corresponding signals. Under these assumptions and from (29) to (32), the constants in (25) and (26) can be chosen as $K_{d1} = 0.04$, $K_{d2} = 37.23$, $K_{q1} = 0.04$, $K_{q2} = 28.87$.

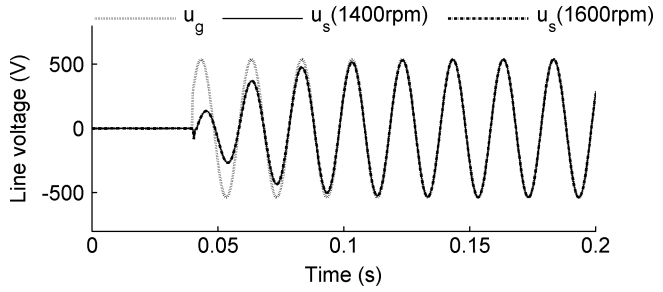

Fig. 3. Simulated grid and stator line voltages with PI control.

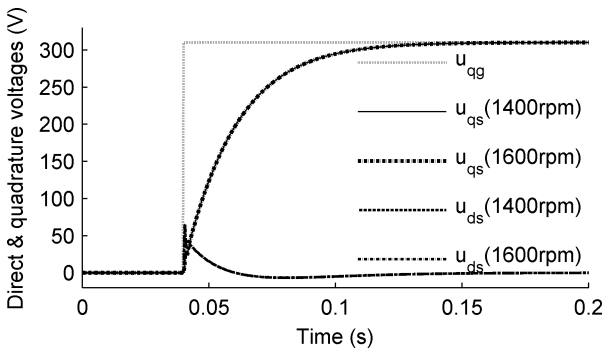

Fig. 4. Simulated grid, stator direct, and quadrature voltages with PI control.

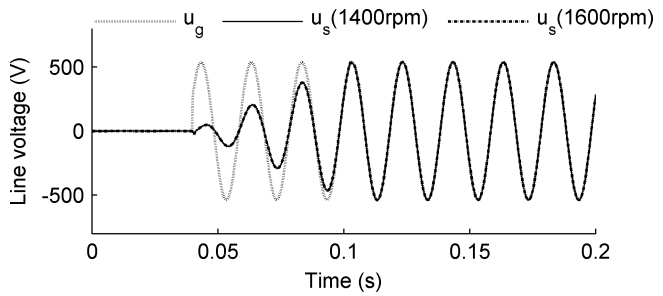

Fig. 5. Simulated grid and stator line voltages with IVSC.

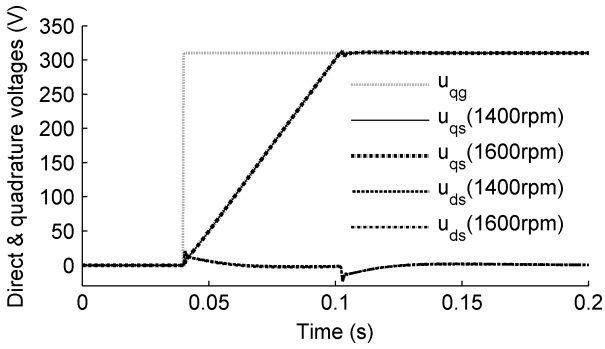

Fig. 6. Simulated grid, stator direct, and quadrature voltages with IVSC.

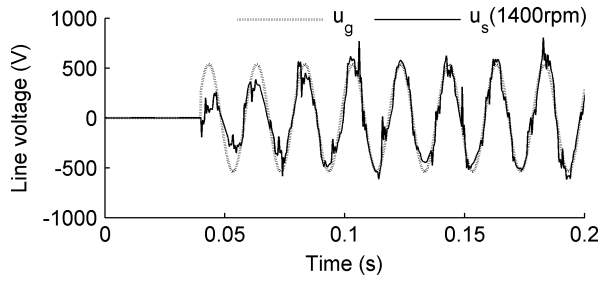

Fig. 7. Simulated grid and stator line voltages with PI control under disturbances.

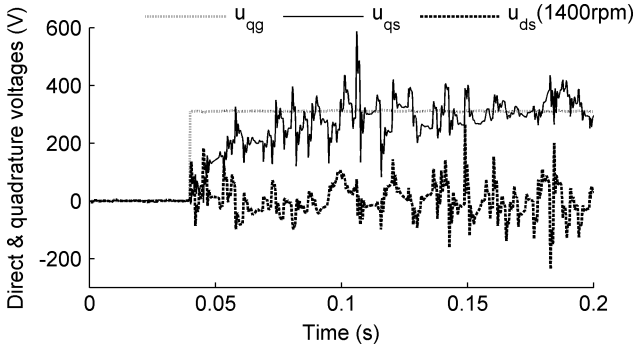

Fig. 8. Simulated grid, stator direct, and quadrature voltages with PI control under disturbances.

A conventional cascaded PI control scheme is also simulated for comparison. The inner loop controllers are tuned to have a close-loop time constant of 0.002 s, and the outer loop controllers are tuned to have a close-loop time constant of 0.02 s.

The grid voltage is applied at time equal to 0.04 s. The grid and stator line voltages of the DFIG with cascaded PI control are shown in Fig. 3 at rotor speed of 1400 and 1600 rpm, respectively, and the corresponding direct and quadrature voltages are shown in Fig. 4. The identical type voltages with proposed IVSC are shown in Figs. 5 and 6. Under both control schemes, the stator voltage tracks the grid voltage rapidly and has its amplitude, frequency, and phase equalized to those of the grid voltage in several periods. It verifies that the conventional cascaded PI control and the proposed IVSC scheme are capable of synchronizing the DFIG at both subsynchronous and supersynchronous speed.

To compare the robustness of the cascaded PI control and the proposed IVSC schemes, white noise with a power spectral density of 0.005 (unit) is added to the measured current and voltage signals. The grid and stator line voltages of the DFIG with cascaded PI control are shown in Fig. 7, and the corresponding direct and quadrature voltages are shown in Fig. 8. The identical type voltages with proposed IVSC are shown in Figs. 9 and 10. In Figs. 7 and 8, the stator voltages of the DFIG contain large-amplitude high-frequency noises when conventional cascaded PI control is used. Figs. 9 and 10 shows that the proposed IVSC can suppress the noise and has better robustness. Figs. 7–10 only display the voltage responses at subsynchronous speed, and the voltage responses at supersynchronous speed are very similar.

To show the parametric robustness of the proposed IVSC scheme, the rotor winding resistance of the DFIG is change to 50% and 150% of nominal value, respectively. The grid and stator line voltages of the DFIG are shown in Fig. 11, and the corresponding direct and quadrature voltages are shown in Fig. 12. The rotor self-inductance of the DFIG is also change to 50%

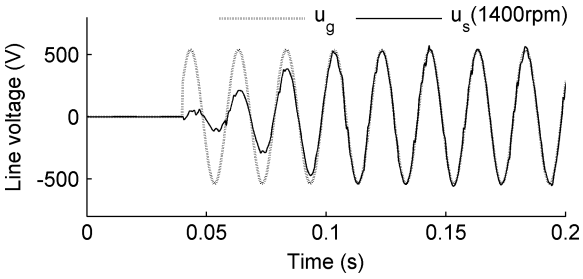

Fig. 9. Simulated grid and stator line voltages with IVSC under disturbances.

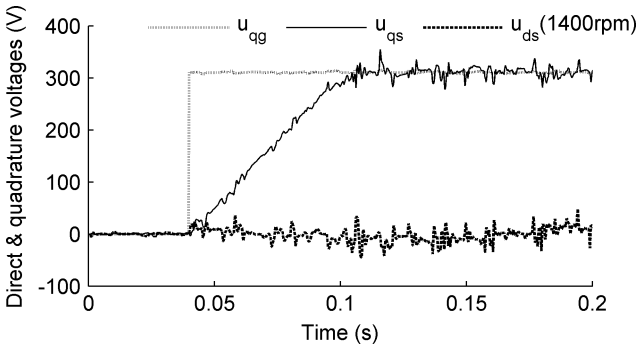

Fig. 10. Simulated grid, stator direct, and quadrature voltages with IVSC under disturbances.

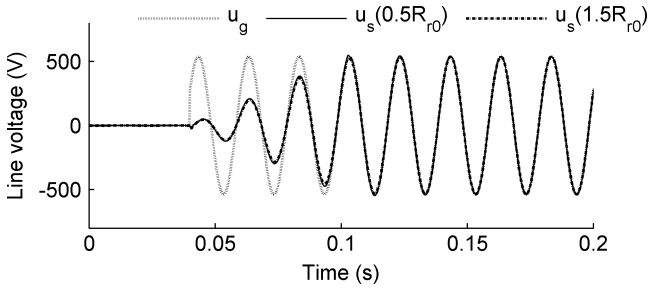

Fig. 11. Simulated grid and stator line voltages with rotor resistance errors.

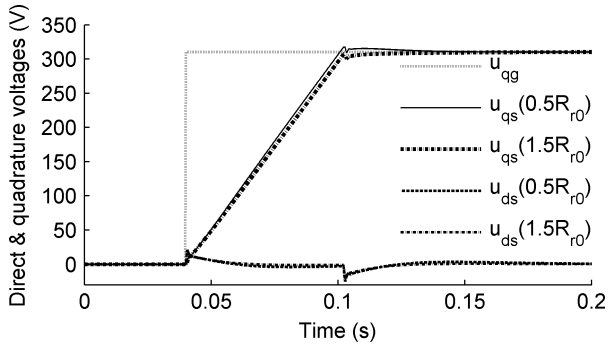

Fig. 12. Simulated grid, stator direct, and quadrature voltages with rotor resistance errors.

and 150% of nominal value, respectively, and the simulation results are shown in Figs. 13 and 14. The responses shown in Figs. 11–14 are almost the same with the responses shown in Figs. 5 and 6, and the parametric robustness of the proposed IVSC scheme is verified.

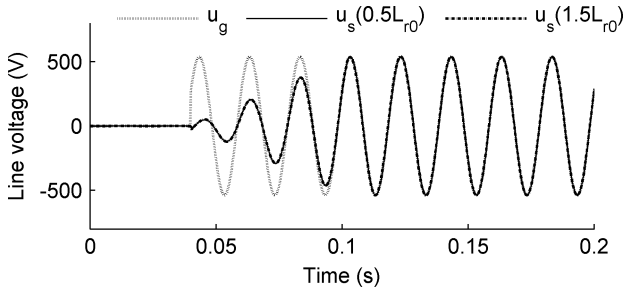

Fig. 13. Simulated grid and stator line voltages with rotor selfinductance errors.

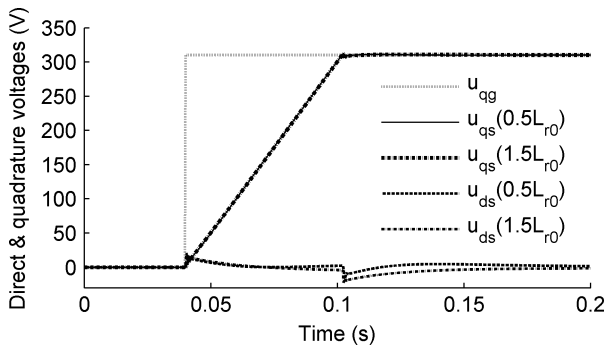

Fig. 14. Simulated grid, stator direct, and quadrature voltages with rotor self-inductance errors.

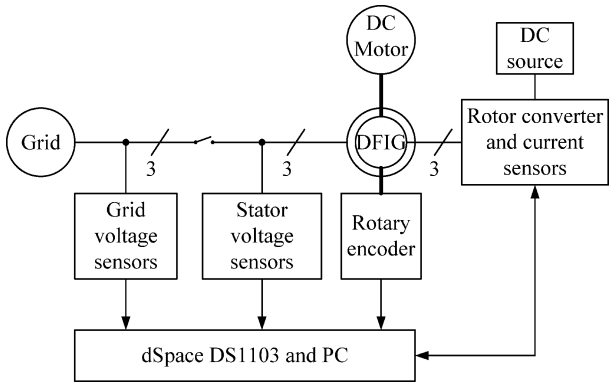

Fig. 15. Configuration of experimental system.

VII. Hardware Experimental Results

Fig. 15 shows the configuration of the experiment system. The rotor speed of the DFIG can be regulated by manually adjusting the voltage applied to the coupled dc motor. The rotor converter is an integrated power module (IPM)-based inverter controlling the voltage applied to the rotor winding of the DFIG. The grid voltage, stator voltage, rotor current, and rotor position are sampled by the prototyping card dSpace DS1103 at a rate of 5 kHz. The prototyping card processes the acquired signals with different algorithms and generates 10 kHz PWM switching signal for the IPM control. The operating conditions and signals are displayed and stored in the personal computer in which the prototyping card is installed.

All the parameters, constants, and variables in hardware experiment are the same as those in simulation. The grid and stator

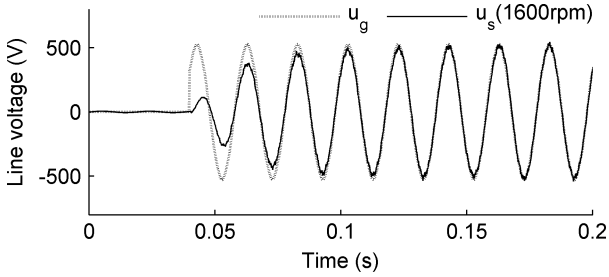

Fig. 16. Grid and stator line voltages with PI control.

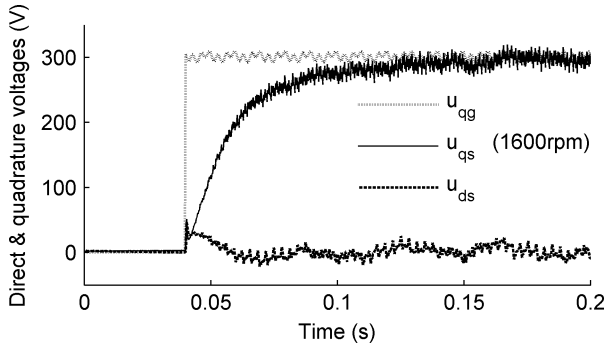

Fig. 17. Grid, stator direct, and quadrature voltages with PI control.

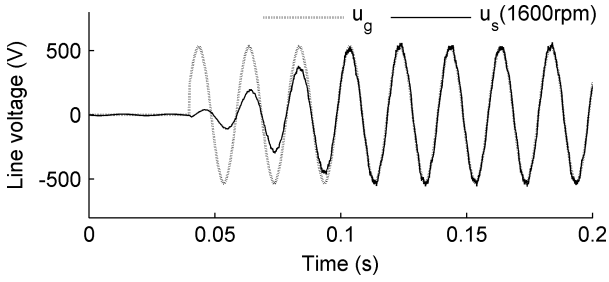

Fig. 18. Grid and stator line voltages with IVSC.

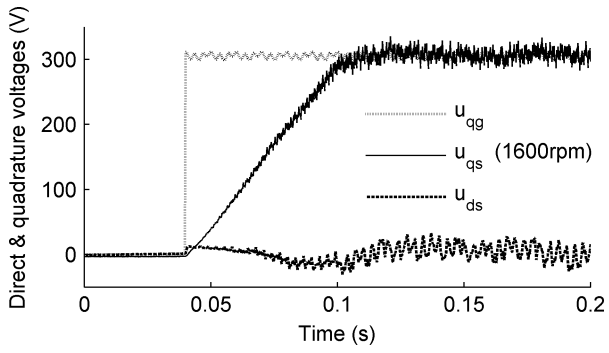

Fig. 19. Grid, stator direct, and quadrature voltages with IVSC.

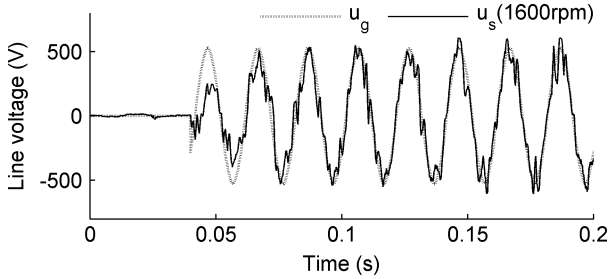

Fig. 20. Grid and stator line voltages with PI control under disturbances.

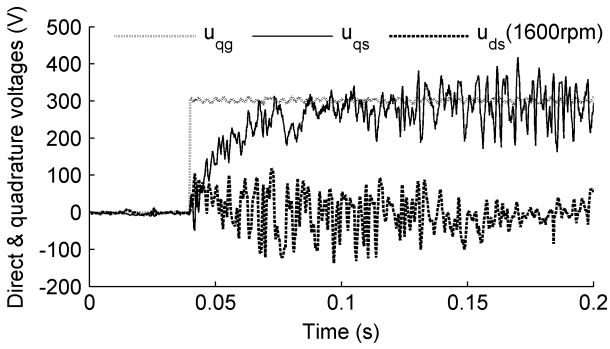

Fig. 21. Grid, stator direct, and quadrature voltages with PI control under disturbances.

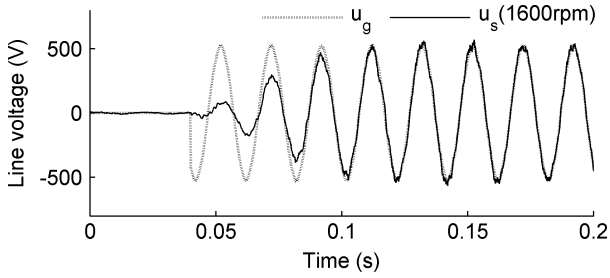

Fig. 22. Grid and stator line voltages with IVSC under disturbances.

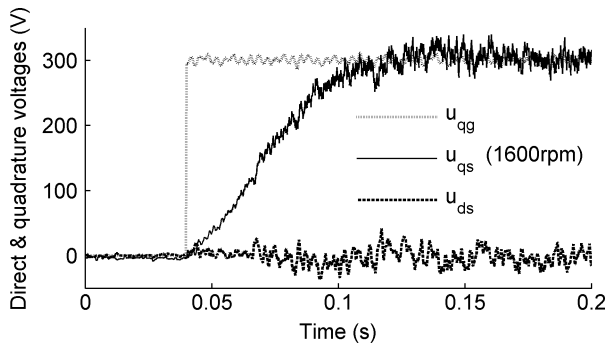

Fig. 23. Grid, stator direct, and quadrature voltages with IVSC under disturbances.

line voltages of the DFIG with cascaded PI control are shown in Fig. 16, and the corresponding direct and quadrature voltages are shown in Fig. 17. The identical type voltages with proposed IVSC are shown in Figs. 18 and 19. White noise with a power spectral density of 0.005 (unit) is added to the measured current and voltage signals, and the stator voltages of the DFIG contain large-amplitude high-frequency noises when cascaded PI control is used (Figs. 20 and 21), and this problem is solved by the proposed IVSC (Figs. 22 and 23). Figs. 16–23 only display the voltage responses at supersynchronous speed, and the voltage responses at subsynchronous speed are very similar.

The harmonic spectra of the stator line voltage of the DFIG without disturbances are shown in Fig. 24. The cascaded PI con-

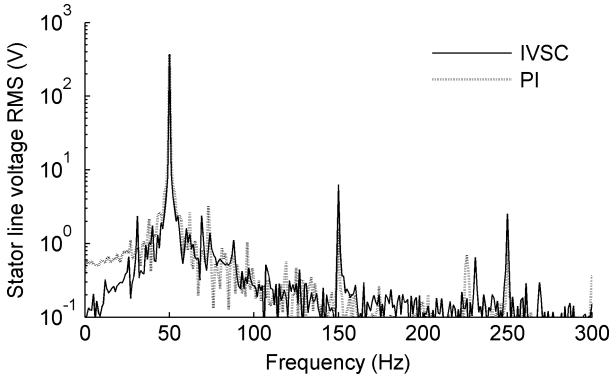

Fig. 24. Harmonic spectrum of the stator line voltage.

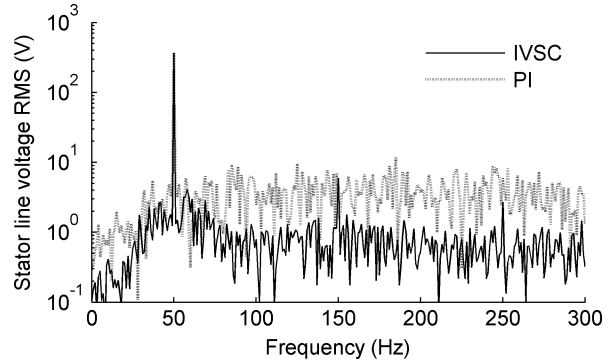

Fig. 25. Harmonic spectrum of the stator line voltage under disturbances.

trol and proposed IVSC scheme have similar harmonic spectra. The dominant frequency of the stator voltage is 50 Hz, which is the same as the grid frequency. When the white noise is added, the proposed IVSC leads to better performance than cascaded PI control, as shown in Fig. 25.

VIII. Conclusion

This paper presents a direct voltage control scheme, using integral variable structure control for the synchronization of the DFIG-based WECS to the power grid. Different from conventional cascaded PI control schemes, parametric uncertainty and external disturbances are formally included into the design procedure of the proposed scheme and hence the robustness of system can be guaranteed.

Simulation and experiment are carried out to compare the performance of conventional cascaded PI control scheme and proposed control scheme. The results show that proposed control scheme has better robustness. The DVC scheme using IVSC is an effective algorithm to synchronize the DFIG-based WECS to the power grid rapidly, even if parametric errors and external disturbances are present.

Appendix

Machine Parameters

Stator rated voltage: 380 V
Stator rated current: 4.5 A
Rotor rated voltage: 120 V
Rotor rated current: 10 A
Operating frequency: 50 Hz
Synchronous speed: 1500 RPM
Magnetizing inductance (referred to the stator): 0.2987 H
Rotor leakage inductance (referred to the stator): 0.0186 H
Stator leakage inductance: 0.0186 H
Rotor winding resistance (referred to the stator): 5.8985 Ω
Stator winding resistance: 2.6596 Ω
Stator-to-rotor turn ratio: 3.1667

Acknowledgment

The authors would like to thank the contributions of K. F. Wong, W. W. Chan, and C. K. Cheung on the experimental setup or their technical support/advices.

References

[1] M. V. A. Nunes, J. A. P. Lopes, H. H. Zurn, H. U. Bezerra, and R. G. Almeida, "Influence of the variable-speed wind generators in transient stability margin of the conventional generators integrated in electrical grids," *IEEE Trans. Energy Convers.*, vol. 19, no. 4, pp. 692–701, Dec. 2004.

[2] A. Petersson, T. Thiringer, L. Harnefors, and T. Petru, "Modeling and experimental verification of grid interaction of a DFIG wind turbine," *IEEE Trans. Energy Convers.*, vol. 20, no. 4, pp. 878–886, Dec. 2005.

[3] A. Petersson, L. Harnefors, and T. Thiringer, "Evaluation of current control methods for wind turbines using doubly-fed induction machines," *IEEE Trans. Power Electron.*, vol. 20, no. 1, pp. 227–235, Jan. 2005.

[4] R. Pena, J. C. Clare, and G. M. Asher, "Doubly fed induction generator using back-to-back PWM converters and its application to variable-speed wind-energy generation," *Inst. Elect. Eng. Proc. Elect. Power Appl.*, vol. 143, no. 3, pp. 231–241, May 1996.

[5] A. Tapia, G. Tapia, J. X. Ostolaza, and R. J. Saenz, "Modeling and control of a wind turbine driven doubly fed induction generator," *IEEE Trans. Energy Convers.*, vol. 18, no. 5, pp. 194–204, Jun. 2003.

[6] G. F. Yuan, J. Y. Chai, and Y. D. Li, "Vector control and synchronization of doubly fed induction wind generator system," in *Proc. 2004 Int. Power Electron. Motion Control Conf.*, pp. 886–890.

[7] L. Morel, H. Godfroid, A. Mirzaian, and J. M. Kauffmann, "Double-fed induction machine: Converter optimisation and field oriented control without position sensor," *Inst. Elect. Eng. Proc. Elect. Power Appl.*, vol. 145, no. 4, pp. 360–368, Jul. 1998.

[8] J. Park, K. Lee, and D. Kim, "Control method of a doubly-fed induction generator with automatic grid synchronization," in *Proc. 2006 IEEE Ind. Electron. Conf.*, pp. 4254–4259.

[9] K. C. Wong, S. L. Ho, and K. W. E. Cheng, "Direct voltage control for grid synchronization of doubly-fed induction generators," *Electr. Power Compon. Syst.*, vol. 36, no. 9, pp. 960–976, Sep. 2008.

[10] I. Erlich, W. Winter, and A. Dittrich, "Advanced grid requirements for the integration of wind turbines into the German transmission system," in *Proc. 2006 IEEE Power Eng. Soc. Gen. Meet.*, p. 1709340.

[11] V. I. Utkin, J. Güldner, and J. X. Shi, *Sliding Mode Control in Electromechanical Systems*. Boca Raton, FL: CRC Press, 1999, pp. 115–130.

[12] S. K. Chung, J. H. Lee, J. W. Park, J. S. Ko, and M. J. Youn, "Current control of voltage-fed PWM inverter for AC machine drives using integral variable structure control," in *Proc. 1995 IEEE Ind. Electron., Control, Instrum. Conf.*, pp. 668–673.

[13] I. Munteanu, S. Bacha, A. Bratcu, J. Guiraud, and D. Roye, "Energy-reliability optimization of wind energy conversion systems by sliding mode control," *IEEE Trans. Energy Convers.*, vol. 23, no. 3, pp. 975–985, Sep. 2008.

[14] P. E. Vidal, M. P. David, and F. Bonnet, "Mixed control strategy of a doubly fed induction machine," *Electr. Eng.*, vol. 90, no. 5, pp. 337–346, May 2008.

[15] Z. Xu and M. F. Rahman, "Direct torque and flux regulation of an IPM synchronous motor drive using variable structure control approach," *IEEE Trans. Power Electron.*, vol. 22, no. 6, pp. 2487–2498, Nov. 2007.

Si Zhe Chen was born in Shantou, China, in 1981. He received the B.Sc. degree in electromechanical engineering from South China University of Technology, Guangzhou, China, in 2005. He is currently working toward the Ph.D. degree at the College of Electric Power, South China University of Technology, Guangzhou, China.

He is also currently working as a Research Assistant at the Department of Electrical Engineering, The Hong Kong Polytechnic University, Kowloon, Hong Kong. His current research interests include control and power electronics technology in renewable energy.

Norbert C. Cheung (S'85–M'91–SM'05) received the B.Sc. degree from the University of London, London, U.K., in 1981, the M.Sc. degree from The University of Hong Kong, Hong Kong, in 1987, and the Ph.D. degree from The University of New South Wales, Kensington, NSW, Australia, in 1995.

He is currently with the Department of Electrical Engineering, The Hong Kong Polytechnic University, Kowloon, Hong Kong. His current research interests include motion control, actuators design, and power electronic drives.

Ka Chung Wong was born in Hong Kong, 1981. He received the B.Eng. degree in electrical engineering and the M.Eng. degree, in 2004, from The Hong Kong Polytechnic University, Kowloon, Hong Kong, where he is currently working toward the Ph.D. degree.

He is also currently a Tutor in The Hong Kong Polytechnic University. His current research interests include control and drives for variable speed power generation.

Jie Wu graduated from the Department of Electric Power, Harbin Institute of Technology, Harbin, China.

He is currently a Professor and a Doctoral Supervisor of the College of Electric Power, South China University of Technology, Guangzhou, China. his current research interests include the field of green energy sources and ecologic environment controls.